HYDROLOGICAL PROCESSES
Hydrol. Process. **30**, 972–985 (2016)
Published online 15 October 2015 in Wiley Online Library
(wileyonlinelibrary.com) DOI: 10.1002/hyp.10685

Energy partitioning over a semi-arid shrubland in northern China

X. Jia,[1,2,3] T. S. Zha,[1,2]* J. N. Gong,[3] B. Wu,[1,2] Y. Q. Zhang,[1,2] S. G. Qin,[1,2] G. P. Chen,[4] W. Feng,[1,2] S. Kellomäki[3] and H. Peltola[3]

[1] *Yanchi Research Station, School of Soil and Water Conservation, Beijing Forestry University, Beijing 100083, China*
[2] *Key Laboratory of soil and Water Conservation and Desertification Combating, Ministry of Education, Beijing Forestry University, Beijing 100083, China*
[3] *School of Forest Sciences, Faculty of Science and Forestry, University of Eastern Finland, Joensuu 80101, Finland*
[4] *Institute for Forest Sciences, Bailongjiang Forestry Management Bureau, Wudu 746010, China*

Abstract:

During the last decade, the widely distributed shrublands in northern China have shown significant signs of recovery from desertification, the result of widespread conservation practices. However, to support the current efforts in conservation, more knowledge is needed on surface energy partitioning and its biophysical controls. Using eddy-covariance measurements made over a semi-arid shrubland in northwest China in 2012, we examined how surface energy-balance components vary on diurnal and seasonal scales, and how biophysical factors control bulk surface parameters and energy exchange. Sensible heat flux (H) exceeded latent heat flux (λE) during most of the year, resulting in an annual Bowen ratio (β, i.e. $H/\lambda E$) of 2.0. λE exceeded H only in mid-summer when frequent rainfall co-occurred with the seasonal peak in leaf area index (*LAI*). Evapotranspiration reached a daily maximum of 3.3 mm day^{-1}, and summed to 283 mm yr^{-1}. The evaporative fraction (*EF*, i.e. $\lambda E/R_n$), Priestley–Taylor coefficient (α), surface conductance (g_s) and decoupling coefficient (Ω) were all positively correlated with soil water content (*SWC*) and *LAI*. The direct enhancement of λE by high vapour pressure deficit (*VPD*) was buffered by a concurrent suppression of g_s. The g_s played a direct role in controlling *EF* and α by mediating the effects of *LAI*, *SWC* and *VPD*. Our results highlight the importance of adaptive plant responses to water scarcity in regulating ecosystem energy partitioning, and suggest an important role for revegetation in the reversal of desertification in semi-arid areas. Copyright © 2015 John Wiley & Sons, Ltd.

KEY WORDS canopy conductance; energy balance; evapotranspiration; Mu Us Desert; shrub; water stress

Received 9 May 2015; Accepted 5 September 2015

INTRODUCTION

The response of ecosystem energy partitioning to climate change is a major concern to ecologists because of local and regional feedbacks to climate, which in turn affects ecosystem carbon and hydrological cycles (Krishnan *et al.*, 2012). Evaportranspiration (*ET*), which corresponds to the latent heat flux (λE), is closely linked to ecosystem productivity (Aires *et al.*, 2008). The energy exchange between the biosphere and atmosphere is controlled by complex interactions among many environmental (e.g. solar radiation, temperature and moisture) and biological (e.g. plant functional type, phenology and stomatal regulation) factors (Ding *et al.*, 2013; Tang *et al.*, 2014). Existing studies have demonstrated that the relative roles of biophysical variables can vary among ecosystem types (Li *et al.*, 2009). For example, in mesic forests and grasslands, shoot growth strongly controls energy partitioning via its impacts on eco-physiological processes (e.g. transpiration), surface albedo and roughness (Hammerle *et al.*, 2008). In boreal and alpine conditions, seasonally low radiation and temperature are key factors limiting the energy dissipated as λE (Launiainen, 2010). In comparison, arid and semi-arid areas are characterized by sporadic precipitation, sparse vegetation and dry soils (Li *et al.*, 2006; Jia *et al.*, 2014). In such environments, the spatio-temporal variability of water availability strongly affects the dynamics of surface energy exchange (Li *et al.*, 2006). However, previous studies have not yet produced a consistent functional pattern for the responses of energy partitioning (e.g. the evaporative fraction, *EF*, and the Bowen ratio, β) and bulk canopy parameters (e.g. surface conductance, g_s, and the decoupling coefficient, Ω) to biophysical controls (Ding *et al.*, 2013). Therefore, a better understanding of the biophysical controls on ecosystem energy partitioning

*Correspondence to: T. S. Zha, Yanchi Research Station, School of Soil and Water Conservation, Beijing Forestry University, Beijing 100083, China.
E-mail: tianshanzha@bjfu.edu.cn

is required for proper assessment of regional and global carbon budget under changing climate (Zha *et al*., 2013).

Arid and semi-arid ecosystems, covering over 40% of the terrestrial surface, are expected to be highly sensitive to climate and land-use changes (Asner *et al*., 2003; Jia *et al*., 2014). Recent experimental studies have revealed a significant potential for dryland ecosystems to sequester atmospheric CO_2 (Gao *et al*., 2012; Jia *et al*., 2014; Poulter *et al*., 2014). However, the energy exchange and partitioning, which are closely coupled to carbon uptake, are far less well studied in these areas (Krishnan *et al*., 2012). In particular, the determination of major factors affecting energy partitioning can help predict how dryland ecosystems may respond to climatic variability and its associated extremes (e.g. increases in drought duration and frequency) (Baldocchi and Xu, 2007). In addition, measurements of the seasonal trends of bulk canopy parameters (e.g. the Priestley–Taylor coefficient, α) and their biophysical controls for water-limited vegetation can be further used to better parameterize and validate eco-hydrological models (Ding *et al*., 2013).

The arid and semi-arid shrublands of northern China, which represent an important land-cover type in Eurasia, are subject to increasing temperature and an altered precipitation pattern (Liu *et al*., 2011; Gao *et al*., 2012). Endemic shrub species are widely used in this vast region for restoration, as they effectively reduce wind erosion (Wang *et al*., 2014). The south edge of the Mu Us Desert in northern China is a critical ecotone between arid and semi-arid climates, and between agricultural and pastoral land use. From the mid-20th century, human disturbances, especially overgrazing and inadequate reclamation, have caused severe vegetation degradation and desertification problems in this area (Chen and Duan, 2009). However, ecosystems have been recovering from desertification since the 1990s when large-scale conservation practices (e.g. fencing and revegetation with shrubs) were put into action (Wang *et al*., 2014). The successful reversal of desertification is evidenced by increased vegetation cover, biodiversity and soil nutrient content (Chen and Duan, 2009). In particular, the growth and expansion of xerophytic shrub species (e.g. *Artemisia ordosica*, *Hedysarum mongolicum* and *Hedysarum scoparium*) have been found in the restoring area of the Mu Us Desert.

Based on both *in situ* measurements and model simulations, shrubs play an important role in the regional carbon and hydrological cycles of northern China (Bourque and Hassan, 2009; Jia *et al*., 2014). So far, however, few (if any) studies have formally examined the biophysical controls of surface energy partitioning (*EF* and β) and the associated bulk surface parameters (g_s, Ω and α) in these shrub-dominated ecosystems. Similarly, the dynamics of energy exchange have not yet been assessed in relation to key biophysical controls, although these ecosystems have been predicted to be extremely sensitive to environmental changes (Gao *et al*., 2012; Jia *et al*., 2014). In a shrub-dominated ecosystem, both environmental factors and biological soil crusts have been observed to affect the seasonal dynamics of soil respiration (Feng *et al*., 2014; Wang *et al*., 2014). Furthermore, eddy-covariance (EC) measurements on the same shrubland revealed that the ecosystem was a net carbon sink of $77\,g\,C\,m^{-2}\,yr^{-1}$ in 2012 (Jia *et al*., 2014).

As a follow-up study to Jia *et al*. (2014), which reported the carbon balance of a shrub-dominated ecosystem in northwest China, we here focus on energy fluxes and their biophysical controls. By analysing EC data collected throughout 2012, we aimed to (1) assess how surface energy balance components varied on diurnal and seasonal scales, (2) examine how net radiation was partitioned among different energy components at varying timescales, and (3) evaluate how seasonal variations in energy partitioning and bulk canopy parameters were related to biophysical factors. In particular, we addressed the biophysical controls over *EF*, β, α, g_s and Ω. We hypothesized that soil moisture and canopy phenology exert the most important surface controls over energy partitioning, and that their effects are mediated by g_s.

MATERIALS AND METHODS

Study site

Energy and water vapour fluxes were measured at the Yanchi Research Station (37°42′31″N, 107°13′37″E, 1530 m a.s.l.), Ningxia, Northwest China. The site is situated at the southern edge of the Mu Us Desert, an area of mid-temperate semi-arid continental climate. The 1954–2004 climate normals from the nearby meteorological station at Yanchi County (~20 km northeast of the study site) report a mean annual temperature of 8.1 °C and a mean annual precipitation (*PPT*) of 287 mm, which is an order of magnitude smaller than the pan-evaporation (2024 mm). Precipitation is highly seasonal (~80% falling during June–September) and shows large interannual variations ($133–572\,mm\,yr^{-1}$). The growing season (May–October) is in phase with the wet period. The soil is sandy with a bulk density of $1.54 \pm 0.08\,g\,cm^{-3}$ (mean ± standard deviation (SD), $n = 16$) in the upper 10 cm of the soil profile. The soil pH ranges between 7.8 and 8.8 (Feng *et al*., 2014). The vegetation is dominated by a mixture of deciduous shrub species (*A. ordosica*, *H. mongolicum* and *H. scoparium*), with scattered distributions of other shrub (*Salix psammophila*) and grass (*Stipa capillata* and *Agropyron cristatum*) species. The canopy height was ~1.4 m in 2012. Roots of dominant

shrubs are distributed mainly in the 20–50 cm soil layer (Wang *et al*., 2014). Water scarcity limits carbon uptake (Jia *et al*., 2014) and soil respiration (Feng *et al*., 2014; Wang *et al*., 2014) at the site.

EC, meteorological and leaf area index (LAI) measurements

The EC system consisted of a sonic anemometer (CSAT3, Campbell Scientific Inc., USA) and a closed-path infrared gas analyser (LI-7200, LI-COR Inc., USA), mounted on a tower at 6.2-m height. Air was drawn from an inlet 20 cm away from the centre of the sonic anemometer sensor volume. The sampled air was then pumped through a tube of 1 m in length and 9 mm in diameter to the LI-7200 at a flow rate of 15 l min^{-1}. On-site maintenance and sensor calibrations were performed periodically. Raw data were sampled at 10 Hz using a data logger (LI-7550, LI-COR Inc., USA). Half-hourly turbulent fluxes were calculated from the covariance between the fluctuations in the vertical wind velocity and the scalar quantities. The underlying surface of the studied shrub ecosystem was flat (slope $< 1°$), and the uniform fetch extended over 250 m in all directions. Ninety percent of the cumulative fluxes originated from within 220 m of the tower.

Meteorological measurements included wind speed (u) and direction (034B, Met One Instruments Inc., USA), net radiation (R_n, CNR-4, Kipp and Zonen, The Netherlands), global shortwave radiation (R_s, CMP-3, Kipp and Zonen, the Netherlands), air temperature (T_a) and relative humidity (RH) (HMP155A, Vaisala, Finland). All these variables were measured at 6-m height on the EC tower. Soil temperature and water content (SWC) were measured at four depths (0.1, 0.3, 0.7 and 1.2 m) at a distance of 10 m from the tower (ECH$_2$O-5TE, Decagon Devices, USA). SWC was calibrated against periodic gravimetric soil moisture measurements. Soil heat flux (G) was calculated as the sum of the heat flux at 10-cm depth ($G_{10\text{-}cm}$), measured at 10 m from the tower using five soil heat flux transducers (HFP01, Hukseflux Thermal Sensors, The Netherlands), and the rate of change in heat storage in the soil layer above the transducers (S_b) (see e.g. Ochsner *et al*., 2007). Rainfall was measured with a manual rain gauge from 15 May to 22 July, and thereafter with a tipping-bucket rain gauge (TE525WS, Campbell Scientific Inc., USA) at a distance of ~50 m from the tower. All meteorological variables were sampled at 0.1 Hz, and the half-hourly values were computed and stored on data loggers (CR200X and CR3000, Campbell Scientific Inc., USA). Additional details on the instrumentation and sampling procedures can be found in Jia *et al*. (2014).

For LAI measurements, 16 quadrats (10 m × 10 m each) were set up in late March 2012 within a 100 m × 100 m plot centred on the EC tower. A hierarchical sampling approach was used for estimating the LAI for each component species. The plot-level LAI was calculated as the sum over all measured species. The sampling was performed at roughly weekly intervals throughout the growing season; see Jia *et al*. (2014) for details.

Data processing and analysis

Calculation of EC fluxes. Post-processing was performed using the EddyPro 4.0.0 software (LI-COR Inc., USA), including spike removal, double coordinate rotation, time delay corrections, frequency response corrections, detrending (block averaging) and flux computation (Burba, 2013). Correction for density fluctuations was not applied because the LI-7200 is capable of outputting mixing ratios (Burba, 2013). Half-hourly fluxes were excluded if missing records, removed spikes or out-of-range values together exceeded 10% of the total records of any variable (e.g. vertical wind velocity, sonic temperature and water vapour mixing ratio) involved in flux calculation. Outliers in half-hourly turbulent fluxes were removed following Papale *et al*. (2006). The friction velocity (u^*) filtering, which is commonly used in screening nighttime carbon fluxes (e.g. Jia *et al*. (2014) used a u^* threshold of 0.18 m s^{-1} at the same site), was not applied here to turbulent energy fluxes. Some authors suggested that the u^* correction may lead to systematic biases in aggregated λE and sensible heat fluxes (H) (Li *et al*., 2006; Launiainen, 2010; Zha *et al*., 2013). Additional analyses (not shown) indicated that the u^* filtering with a threshold of 0.18 m s^{-1} had little effect on our results. The latent heat storage ($S_{\lambda E}$) and sensible heat storage (S_H) terms in the air column below the EC instrument height were estimated following Zha *et al*. (2004), in which the time rates of changes in T_a and water vapour concentration were calculated for a single height (6 m) above the ground.

In 2012, instrument failures, system maintenance and data screening led to a total of 962 missing values (5.5%) in half-hourly λE fluxes, 423 missing values (2.4%) in H, 380 missing values (2.2%) in R_n and 96 missing values (0.6%) in the mean G over the five replicates. All missing values were replaced with estimated values in order to calculate the annual energy budget. Linear interpolation was used to fill small gaps (≤2 h) in the half-hourly flux time series. For larger gaps the mean diurnal variation (MDV) approach was applied to consecutive 15-day windows (see e.g. Krishnan *et al*., 2012). The largest gap was for λE during 4–12 May, as a result of pump failure. Most of the remaining gaps were of several hours or less.

Calculation of bulk surface parameters. Bulk surface parameters, including g_s, Ω and α (see Appendix A for a

list of parameters and abbreviations), were calculated to help investigate the biophysical controls on λE (Liu and Feng, 2012). We estimated g_s ($m\,s^{-1}$) by inverting the Penman–Monteith equation (Monteith, 1965):

$$\lambda E = \frac{\Delta(R_n - G) + \rho C_p VPD g_a}{\Delta + \gamma\left(1 + \frac{g_a}{g_s}\right)} \quad (1)$$

where Δ is the rate of change of saturation vapour pressure with T_a ($kPa\,K^{-1}$), ρ the air density ($kg\,m^{-3}$), C_p the specific heat capacity of air ($J\,kg^{-1}\,K^{-1}$), γ the psychrometric constant ($kPa\,K^{-1}$) and *VPD* the atmospheric vapour pressure deficit (kPa). The aerodynamic conductance (g_a, $m\,s^{-1}$) is given by (Monteith and Unsworth, 1990):

$$g_a = \left(\frac{u}{u^{*2}} + 6.2u^{*-0.67}\right)^{-1}. \quad (2)$$

The value of g_s represents the aggregate conductance of dry canopy (transpiration), wet canopy (evaporation) and soil surface (evaporation). However, during the growing season when *ET* comes largely from transpiration, g_s strongly reflects the canopy-integrated stomatal conductance (Liu and Feng, 2012).

Ω was calculated as (Jarvis and McNaughton, 1986):

$$\Omega = \frac{\Delta + \gamma}{\Delta + \gamma\left(1 + \frac{g_a}{g_s}\right)}. \quad (3)$$

Ω is a measure of the degree of coupling between the ecosystem surface and the atmospheric boundary layer. Ω varies from 0 (i.e. canopy surface and the atmosphere are coupled and λE is mostly controlled by g_s and *VPD*) to 1 (i.e. canopy surface and the atmosphere are decoupled and λE is mostly controlled by R_n).

The coefficient α is the ratio of actual λE to the equilibrium λE (λE_{eq}) (Aires *et al.*, 2008). The λE_{eq} was estimated as (Priestley and Taylor, 1972):

$$\lambda E_{eq} = \frac{\Delta(R_n - G)}{\Delta + \gamma}. \quad (4)$$

Usually, $\alpha \geq 1$ can be expected in mesic ecosystems, indicating sufficient water supply so that λE is limited by available energy. In contrast, $\alpha < 1$ has been observed in semi-arid and arid ecosystems where λE is usually water-limited (Liu and Feng, 2012).

Energy partitioning (*EF*, i.e. $\lambda E/R_n$ and β, i.e. $H/\lambda E$) and bulk surface parameters (g_s, Ω and α) were calculated for dry canopy periods only (non-rainy days). To avoid spurious values caused by low solar elevation, we rejected all periods when shortwave incoming radiation was less than $100\,W\,m^{-2}$ (Li *et al.*, 2006).

Statistical analysis. Surface energy-balance closure was evaluated using linear regression as:

$$\lambda E + H - S_a = a_0 + a_1(R_n - G) \quad (5)$$

where S_a is $S_{\lambda E} + S_H$, and G is $G_{10\text{-}cm} + S_b$. Values of $a_0 = 0$ and $a_1 = 1$ indicate perfect energy-balance closure. In addition, S_a and S_b were removed from Equation (5) to assess the contributions of above- and belowground heat storage terms to energy-balance closure.

We also used regression analyses to test the effects of *LAI*, *SWC* and *VPD* on *EF*, α, g_s, Ω and β, and to examine the role of g_s in controlling *EF*, α and g_s. Half-hourly *LAI* values were derived by linearly interpolating between measurements. Response variables were bin-averaged before regressions were conducted, using bins of $0.05\,m^2\,m^{-2}$ for *LAI*, $0.01\,m^3\,m^{-3}$ for *SWC* and 0.2 kPa for *VPD*. For testing the effects of abiotic controls (*SWC* and *VPD*), only data from the mid-growing season (June–August) were used to minimize the confounding effects of canopy phenology. The effects of g_s were assessed for both the whole year and the mid-growing season using bin-averaged values ($0.5\,mm\,s^{-1}$ g_s intervals). All reported relationships were statistically significant ($p < 0.05$).

Path analysis was used to elucidate the direct and indirect effects of biophysical factors (*LAI*, *SWC*, *VPD*, T_a and g_s) on *EF* and α. The direct path coefficient between two variables is the standardized partial-regression coefficient (which varies from -1 to 1) given by multiple regression, and the indirect path coefficient is the product of direct coefficients summed over all paths. The total path coefficient is the sum of direct and indirect coefficients (Tang *et al.*, 2014). Initial models included all potential causalities based on widely accepted knowledge, and final models were derived by removing insignificant ($p \geq 0.05$) paths and recalculating coefficients. The path analysis was applied to daily-resolution data for the growing period ($LAI > 0$).

RESULTS

Seasonal variations in biophysical factors

Daily maximum air temperature (T_{a_max}) ranged from about $-5\,°C$ in winter to $30\,°C$ in summer (Figure 1a). Daily minimum air temperature (T_{a_min}) displayed a similar seasonal trend, varying from -12 to $19\,°C$. Daily R_s increased from about $10\,MJ\,m^{-2}\,day^{-1}$ in January to a maximum of $31.5\,MJ\,m^{-2}\,day^{-1}$ on 15 June (DOY 167), and declined thereafter (Figure 1b). The annual sum of R_s was $6001\,MJ\,m^{-2}$. Daily mean *VPD* reached a maximum of 2.2 kPa in early summer, but was lower than 0.5 kPa in winter (Figure 1c). Rainfall summed to 303 mm from mid-May to December, with over 60% of the total falling

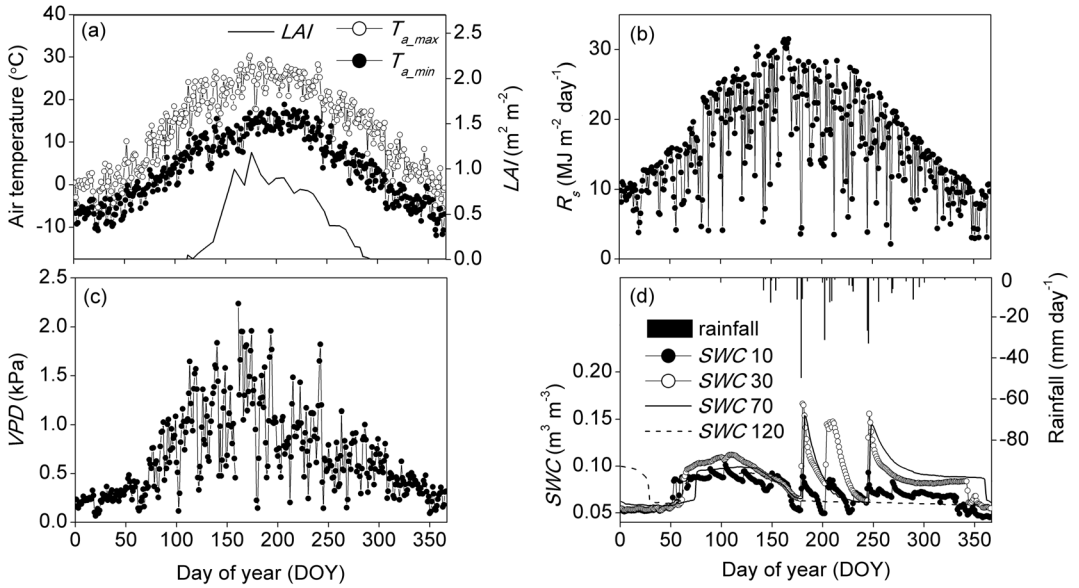

Figure 1. Seasonal variations of (a) daily maximum (T_{a_max}) and minimum (T_{a_min}) temperature at 6 m above the ground and leaf area index (*LAI*), (b) shortwave global solar radiation (R_s), (c) vapour pressure deficit (*VPD*) and (d) soil water content (*SWC*) at four depths (10, 30, 70 and 120 cm) and rainfall in 2012. Daily sums are shown for rainfall and R_s, while daily means are shown for T_{a_max}, T_{a_min}, *VPD* and *SWC*. Linearly interpolated values are shown for *LAI*. *LAI*, *VPD*, *SWC* and rainfall data are from Jia *et al.* (2014)

during June–August (Figure 1d). Summer storms resulted in three large rainfall events (>20 mm day^{-1}). Snowmelt and soil thaw led to a plateau of *SWC* in early spring (DOY 60–150, Figure 1d). During the growing season, *SWC* at shallow depths was frequently replenished by rainfall, whereas *SWC* deep in the profile (120 cm) did not respond to any rainfall event. Canopy development was generally in phase with solar irradiance and the wet period, with *LAI* reaching a maximum of 1.2 m^2 m^{-2} in June (Figure 1a).

Seasonal variations in energy fluxes and bulk surface parameters

Analysis of surface energy-balance closure (Equation (5)) gave coefficients of $a_1 = 0.82$ and $a_0 = 1.40$ W m^{-2}. The analysis was insensitive to the exclusion of S_a ($a_1 = 0.80$, $a_0 = 2.64$ W m^{-2}), but was strongly affected by removing S_b ($a_1 = 0.68$, $a_0 = 12.12$ W m^{-2}).

The seasonal course of daily R_n tracked that of R_s (Figures 1b and 2a), ranging from -0.5 MJ m^{-2} day^{-1} on 9 November (DOY 314) to over 15 MJ m^{-2} day^{-1} in summer. Annual R_n (2548 MJ m^{-2}) corresponded to 43% of annual R_s. Daily G varied from negative values in late autumn and winter (a minimum of -2.4 MJ m^{-2} day^{-1} on 1 September, DOY 245) to about 2 MJ m^{-2} day^{-1} in spring and early summer (Figure 2b). G contributed significantly to the energy balance on daily and seasonal timescales, but summed to near zero annually (0.4% of

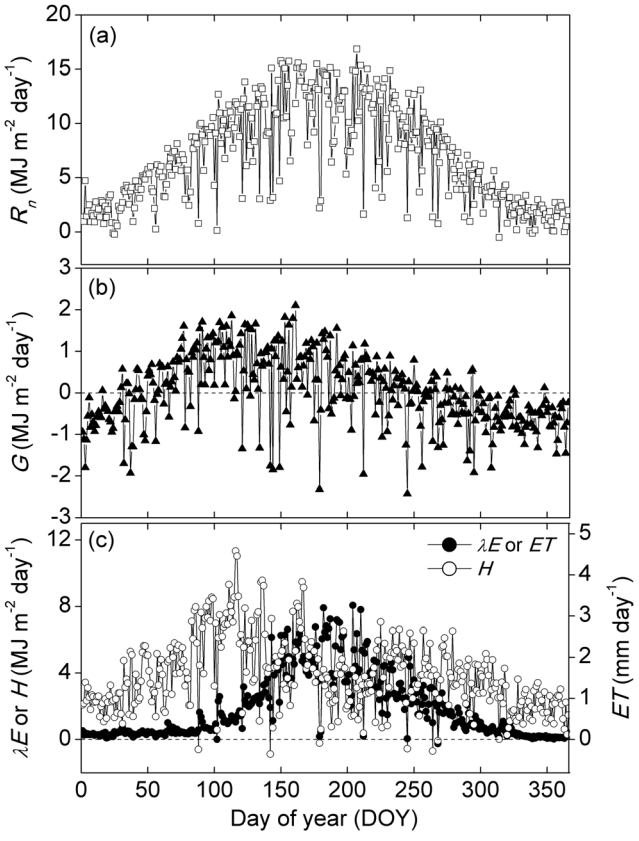

Figure 2. Seasonal pattern of (a) daily net radiation flux (R_n), (b) soil heat flux (G), and (c) sensible heat flux (H) and latent heat flux (λE) in 2012. The dashed lines in (b) and (c) represent zero reference lines

R_n). Daily H showed a bimodal seasonal pattern, with a spring peak of 11.3 MJ m^{-2} day^{-1} on 25 May (DOY 116) and an autumn plateau of about 6.5 MJ m^{-2} day^{-1} during DOY 220–270 (Figure 2c). Daily H was remarkably low on rainy or cloudy days, but it recovered rapidly as the surface dried. H was also low during wintertime (~2 MJ m^{-2} day^{-1}). Cumulative H over the year was 1411 MJ m^{-2}, and the annual H/R_n was 0.55.

Daily λE was smaller than 1 MJ m^{-2} day^{-1} throughout the winter, increased from spring to mid-summer (with a maximum of 7.9 MJ m^{-2} day^{-1}, or an ET equivalent of 3.3 mm day^{-1}), and declined thereafter (Figure 2c). The seasonal peak of λE lagged that of H by about 2.5 months. In addition, λE was greater than H only during a short period in early summer (DOY 170–220). The dynamics of λE were affected by soil dry–wet cycles (Figure 3). Daily λE increased abruptly following large rain events (>20 mm day^{-1}), and then decreased gradually with depleting SWC at 30-cm depth. The large day-to-day variations in λE following storms reflected the effects of other factors (e.g. small rain events, solar radiation and temperature) on λE. The annual sum of λE was 695 MJ m^{-2}, corresponding to an ET of 283 mm yr^{-1} and an annual EF of 0.27. Monthly ET_{eq} reached peak values in summer months (~100 mm mon^{-1}, Table I) and summed to 692 mm yr^{-1}. The ET/PPT ratio, a measure of rain-use efficiency, exceeded 0.90 in mid-summer but fell to 0.43–0.65 during the late growing season (Table I). PPT/ET_{eq}, which is a measure of water supply deficit, ranged from 0.46 to 0.90 during the growing season.

The dry-canopy EF and bulk surface parameters (α, g_s and Ω) showed similar seasonal trends (Figure 4).

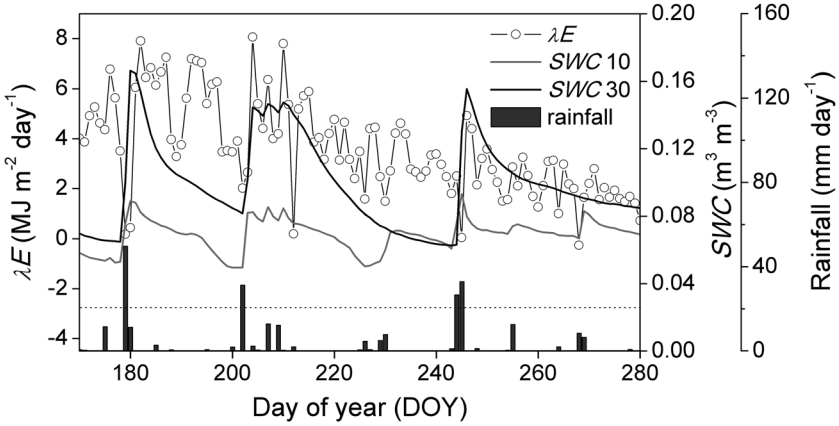

Figure 3. Dynamics of daily latent heat flux (λE) in relation to soil dry–wet cycles caused by rain events. *SWC* 10 and *SWC* 30 represent soil water content at 10-cm and 30-cm depth, respectively. The horizontal dotted line indicates a rainfall intensity of 20 mm day^{-1}

Table I. IMidday (10:00–15:00 h, LST = GMT +8) energy partitioning and monthly water budget over the growing season (GS) of 2012[a]

	Month						
	May	June	July	August	September	October	GS
H/R_n	0.48	0.42	0.30	0.40	0.43	0.56	0.43
G/R_n	0.26	0.21	0.19	0.16	0.19	0.23	0.21
EF	0.21	0.27	0.34	0.24	0.18	0.11	0.23
β	2.29	1.56	0.88	1.67	2.30	5.09	2.3
ET (mm mon^{-1})	39.1	58.8	65.0	43.2	27.7	13.7	237.5
ET_{eq} (mm mon^{-1})	86.44	108.13	106.06	100.75	70.91	44.07	516.35
PPT (mm mon^{-1})		82.6	66.5	46.0	63.9	21.1	
ET/PPT		0.71	0.98	0.94	0.43	0.65	
PPT/ET_{eq}		0.76	0.63	0.46	0.90	0.48	
LAI (m^2 m^{-2})	0.31	0.97	0.88	0.73	0.38	0.05	

[a] R_n, net radiation; G, soil heat flux; H, sensible heat flux; λE, latent heat flux; EF, evaporative fraction ($\lambda E/R_n$); β, Bowen ratio ($H/\lambda E$); ET, evapotranspiration; ET_{eq}, equilibrium ET; PPT, precipitation (available since 15 May 2012); LAI, leaf area index.

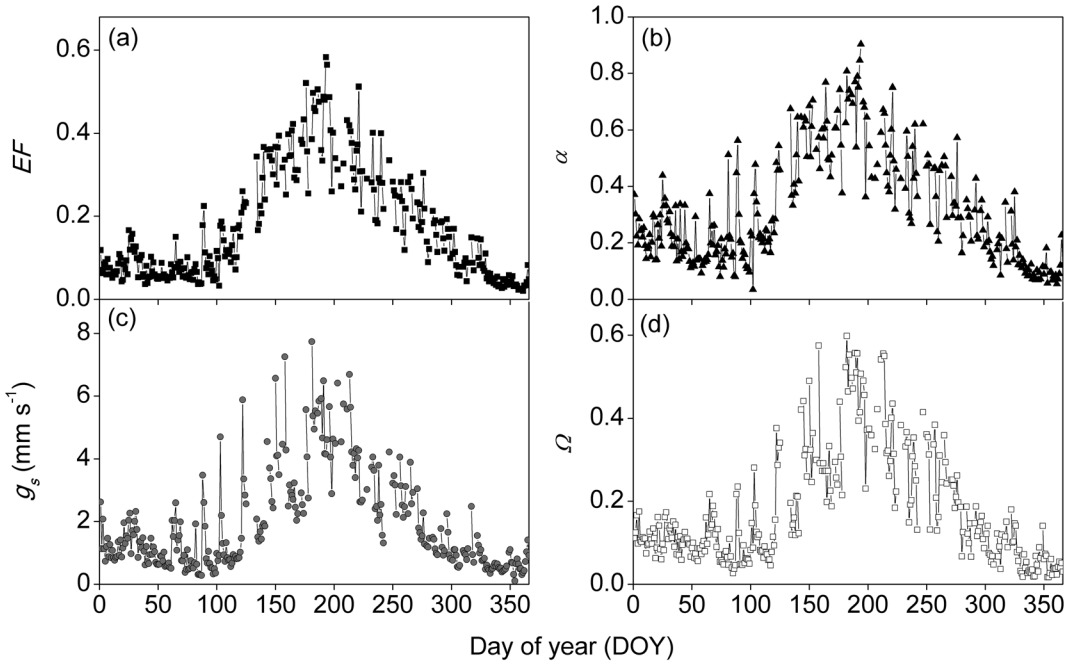

Figure 4. Seasonal pattern of (a) the evaporative fraction (*EF*), (b) Priestley–Taylor coefficient (α), (c) bulk surface conductance (g_s) and (d) decoupling coefficient (Ω) in 2012. Daily means under dry surface conditions (i.e. on non-rainy days) are shown. Only half-hourly values when the shortwave incoming radiation was greater than 100 W m^{-2} were used for calculating daily means in order to avoid spurious values caused by low solar radiation conditions

Their daily mean values were generally close to zero during wintertime, but reached a maximum ($EF = 0.6$, $\alpha = 0.9$, $g_s = 7.7$ mm s^{-1} and $\Omega = 0.6$) in late June or early July.

Diurnal variations in energy fluxes

The upper envelop of R_n ranged from about 250 W m^{-2} in January to over 500 W m^{-2} in July (Figure 5). Both H and G showed clear diurnal variations following the diel cycles of R_n. The diurnal peaks of H and G varied from about 190 and 50 W m^{-2} in winter to 250 and 140 W m^{-2} in spring, respectively. However, λE showed little diurnal variations during the non-growing season, with values close to zero. During the growing season, λE displayed a clear diurnal cycle, with a maximum diurnal peak of 180 W m^{-2} in July (Figure 5c–e). During midday (10:00–15:00), H was generally larger than λE in most months except July, when λE exceeded H and β became <1 (Figure 5 and Table I). For all months except summer, G also exceeded λE (Figure 5 and Table I), highlighting the

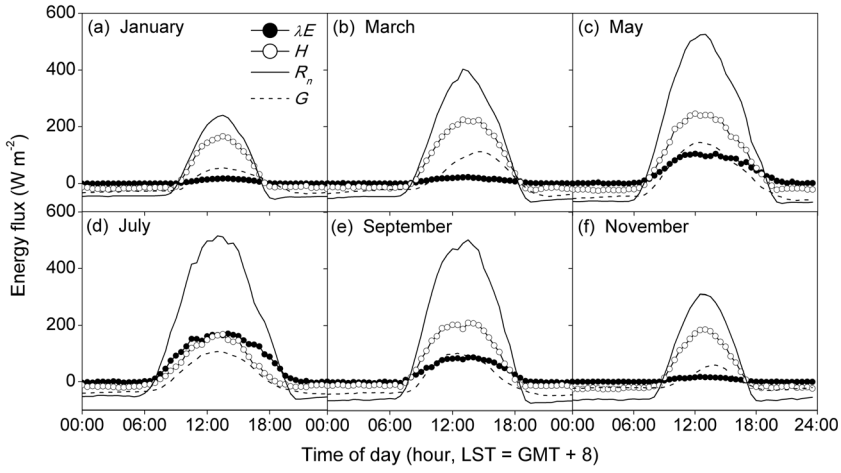

Figure 5. Mean diurnal courses of net radiation flux (R_n), soil heat flux (G), sensible heat flux (H) and latent heat flux (λE) for different months in 2012

large contribution of G to the surface energy balance in semi-arid ecosystems.

Biophysical controls on energy partitioning and bulk surface parameters

Seasonal variations in *LAI* explained 76% of the variability in *EF* and accounted for 36–57% of the variability in bulk surface parameters (Figure 6). During the mid-growing season (June–August), *EF*, g_s α and Ω were all strongly correlated with *SWC* at 30-cm depth (Figure 7). However, these variables were not significantly affected by *SWC* at shallower or deeper layers (data not shown). Both *EF* and α increased with *VPD* up to *VPD* values of 1 kPa, but then levelled off to *EF* and α asymptotes of about 0.38 and 0.6, respectively (Figure 8a–b). g_s increased slightly with *VPD* up to *VPD* of 1 kPa, then decreased from a peak of 5 mm s^{-1} to about 2 mm s^{-1} at *VPD* of 3 kPa (Figure 8c). Ω showed a strong negative correlation with *VPD* (Figure 8d). During the mid-growing season, β decreased exponentially with increasing *SWC* at 30-cm depth, and dropped below 1 when $SWC > 0.09\ m^3\ m^{-3}$ (Figure 9a). Also, β decreased exponentially with increasing *LAI* from about 4 ($LAI = 0.1\ m^2\ m^{-2}$) to 1 ($LAI = 1.2\ m^2\ m^{-2}$), and increased with *VPD* over the range 1–3.5 kPa (Figure 9b and c). *EF*, α and Ω were all tightly correlated with g_s (Figure 10). In addition, the year-round relationships among these variables were non-linear, i.e. with steeper slopes at lower g_s (Figure 10a), whereas the g_s responses of *EF*, α and Ω for the mid-growing season were linear (Figure 10b).

Path analysis revealed strong positive effects of g_s on *EF* and α, with the direct path coefficients exceeding 0.90 (Figure 11). High *VPD* also directly promoted *EF* and α, with a direct path coefficient of 0.52. *LAI* was the main factor controlling g_s, followed by *SWC* and *VPD* whose direct effects on g_s were similar in magnitude but opposite in sign (Figure 11). In addition, high *VPD* indirectly suppressed g_s, via a negative effect on *SWC*. As mediated by g_s, the indirect path coefficients of *LAI*, *SWC* and *VPD* on *EF* (α) were 0.68 (0.66), 0.30 (0.29) and −0.36 (−0.35), respectively. The indirect effects of *VPD* partially offset its direct effects, resulting in a total path coefficient of 0.16 for *EF* and 0.17 for α. Neither *LAI* nor *SWC* showed any significant direct effect on *EF* and α, their indirect path coefficients therefore equaled the total path coefficients. T_a showed a weak direct effect (negative) on α, but not on *EF* (Figure 11).

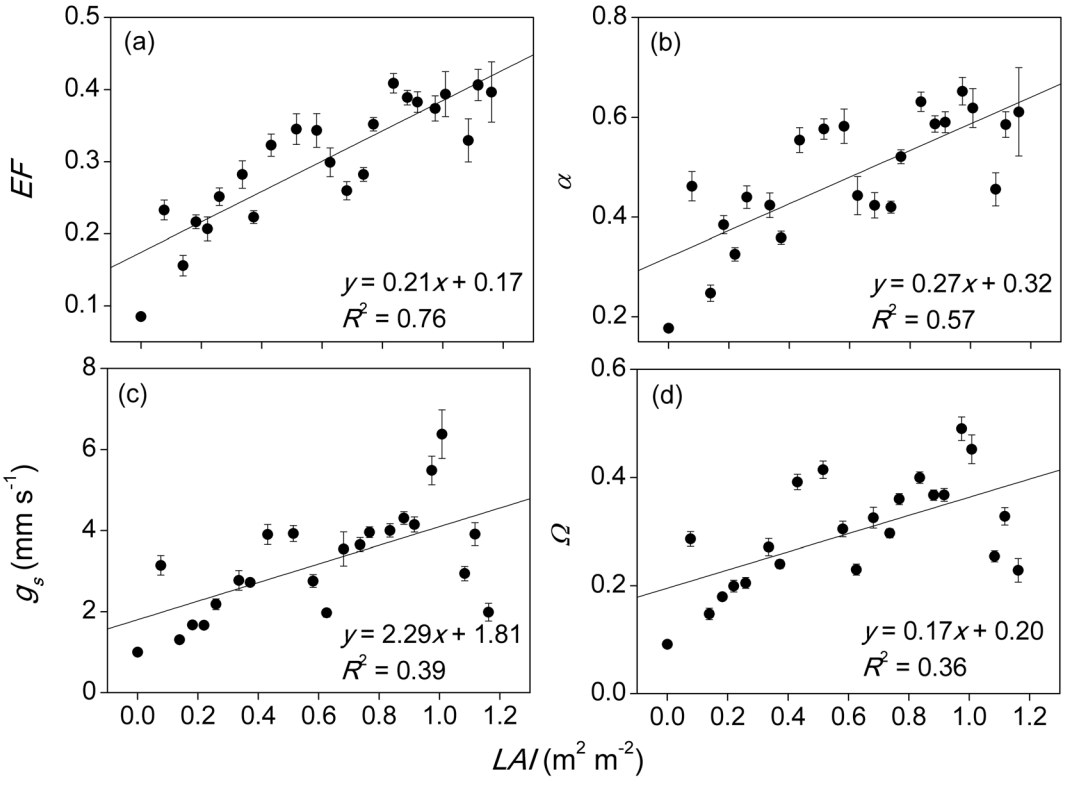

Figure 6. Relationship between leaf area index (*LAI*) and (a) evaporative fraction (*EF*), (b) Priestley–Taylor coefficient (α), (c) bulk surface conductance (g_s) and (d) decoupling coefficient (Ω) in 2012. *LAI* measurements were interpolated to the half-hourly resolution, and then dependent variables were bin-averaged into 0.05 m^2 m^{-2} *LAI* increments. Error bars refer to ±1 standard error

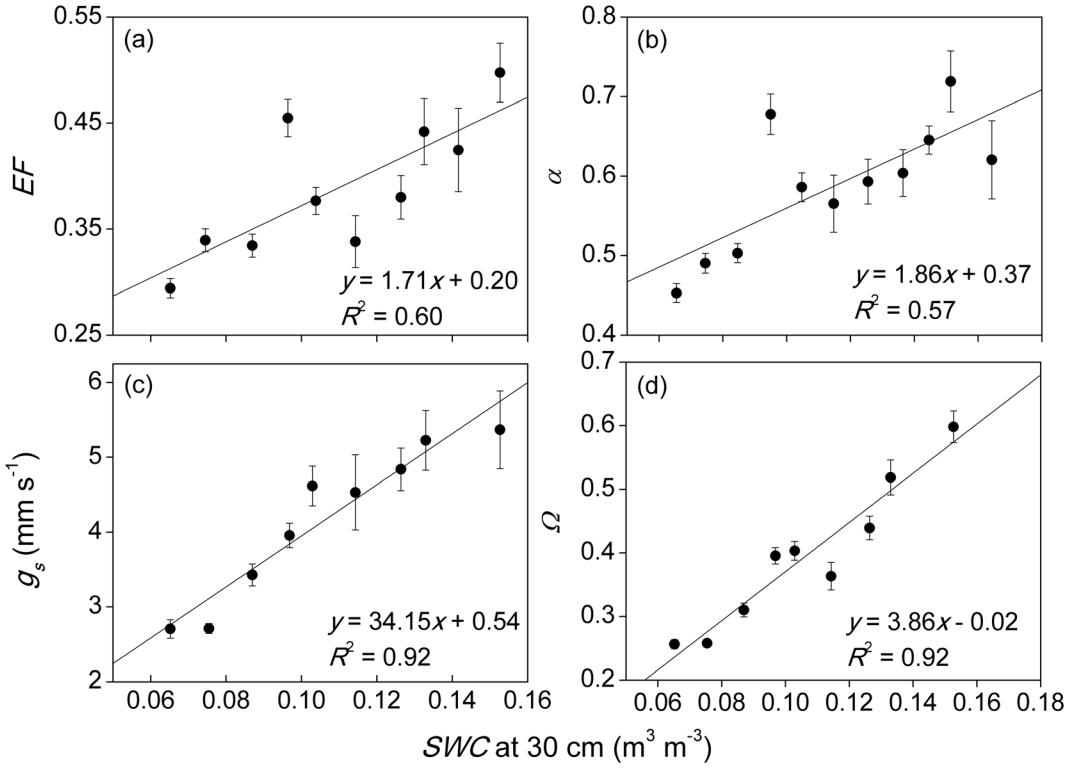

Figure 7. Relationship between soil water content (*SWC*) and (a) evaporative fraction (*EF*), (b) Priestley–Taylor coefficient (α), (c) bulk surface conductance (g_s) and (d) decoupling coefficient (Ω) in 2012. Only data for the mid-growing period (June–August) were used to minimize the confounding effects of canopy phenology. Half-hourly values were bin-averaged into 0.01 $m^3 m^{-3}$ *SWC* increments. Error bars refer to ±1 standard error

DISCUSSION

Energy balance

The surface energy imbalance ($a_1 = 0.82$) fell within the range (0.53–0.99 with a mean of 0.79) reported for FLUXNET sites (Wilson *et al.*, 2002). It should be noted that an imperfect energy balance closure may lead to uncertainties in estimating energy fractions (e.g. *EF*). Although a few studies applied energy-closure adjustments to λE and H, many others did not do so because of the unclear source of energy imbalance (Wilson *et al.*, 2002; Barr *et al.*, 2006). Our results were not qualitatively affected by applying such corrections (data not shown).

The relative importance of different energy-balance components varied with time of year and the timescale considered. On an annual basis, H was the dominant term, and the annual β was 2.0. Seasonally, H exceeded λE during most of the year (Figures 2c and 5 and Table I). Similar β values have been reported for other arid and semi-arid ecosystems where low precipitation, dry soils and a sparse canopy constrain λE (Li *et al.*, 2006; Hao *et al.*, 2007; Aires *et al.*, 2008).

Our results concur with previous studies that reported a large magnitude of G in semi-arid ecosystems (Heusinkveld *et al.*, 2004; Ochsner *et al.*, 2007). They highlight the importance of careful attention to the measurement of G in dryland environments, and to the heat storage term (S_b) in particular. The observed importance of G can be attributed to the low canopy coverage and usually dry soil surface (Gao *et al.*, 2012). Although G showed large diurnal and seasonal variations (Figures 2b and 5), it became negligible at the annual timescale; the annual G/R_n ratio was only 0.4%. Over long timescales, the partitioning of R_n between λE and H has a major impact on local climate and hydrology (Launiainen, 2010).

Daily λE dominated H during mid-summer (Figure 2c) when rainfall was frequent and *LAI* was high (Figure 1a and d). The inverse relationship between λE and H over the growing season (Figure 2c) was consistent with previous observations in semi-arid steppe and shrub ecosystems (Li *et al.*, 2006). Annual *EF* (0.27) was close to that (0.26) reported by Li *et al.* (2006), and fell within the range (0.18–0.29) reported for an undisturbed semi-arid grassland in North American (Krishnan *et al.*, 2012). However, it was lower than that in a

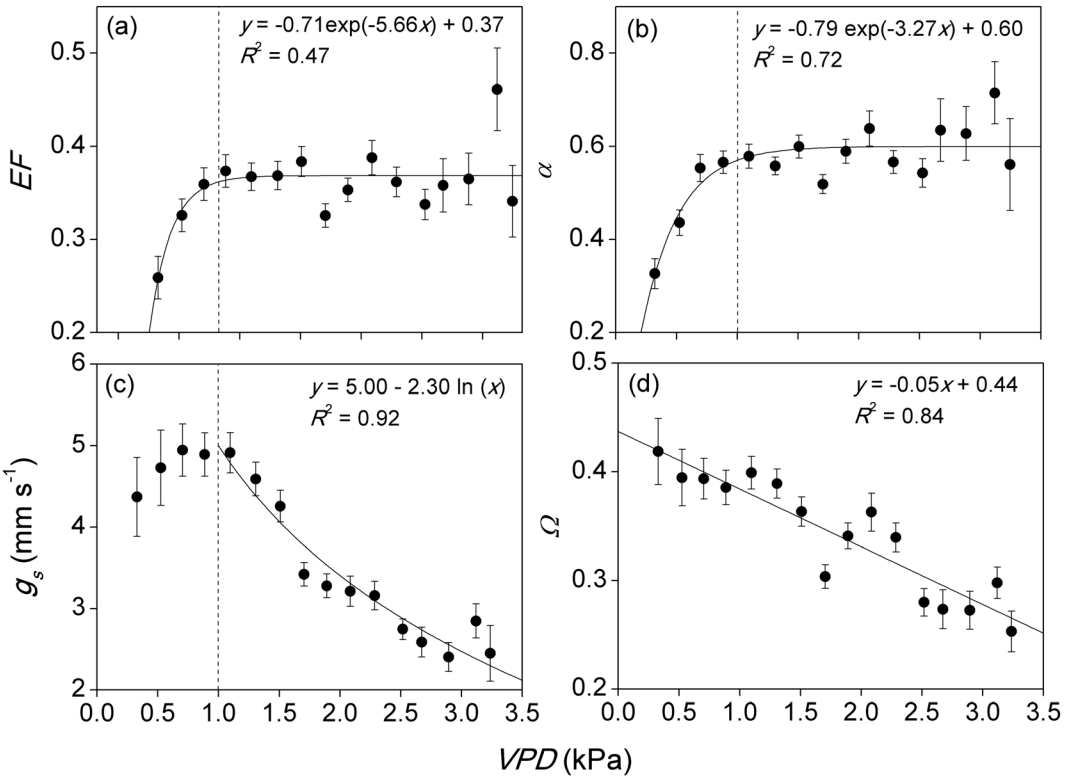

Figure 8. Relationship between vapour pressure deficit (*VPD*) and (a) evaporative fraction (*EF*), (b) Priestley–Taylor coefficient (α), (c) bulk surface conductance (g_s) and (d) decoupling coefficient (Ω) in 2012. Only data for the mid-growing period (June–August) were used to minimize the confounding effects of canopy phenology. Half-hourly values were bin-averaged into 0.2-kPa *VPD* increments. Error bars refer to ±1 standard error. The dashed lines denote $VPD = 1$

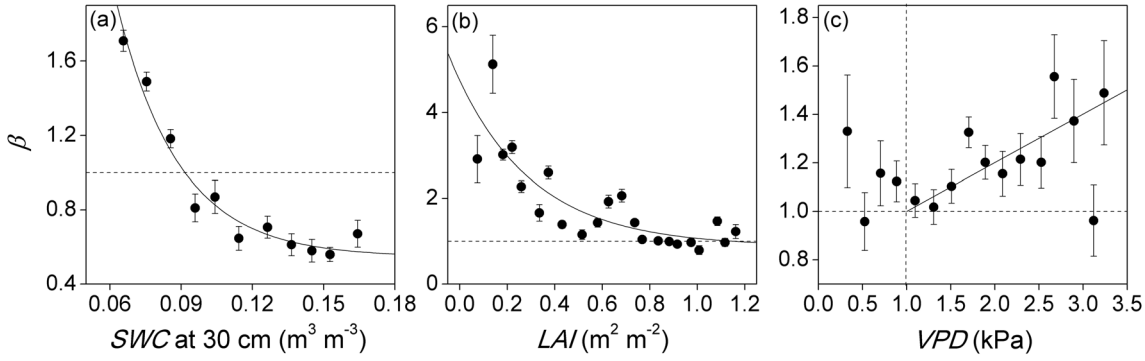

Figure 9. Effects of (a) soil water content (*SWC*), (b) leaf area index (*LAI*) and vapour pressure deficit (*VPD*) on the Bowen ratio (β). The horizontal dashed lines represent $\beta = 1$; the vertical dashed line in (c) denotes $VPD = 1$. In (a) and (c), only data for the mid-growing period (June–August) were used to minimize the confounding effects of canopy phenology. Data when $LAI > 0$ were used in (b). The regression equations are: (a) $y = 15.07\exp(-38.24x) + 0.55$, $R^2 = 0.96$; (b) $y = 3.87\exp(-3.04x) + 0.88$, $R^2 = 0.71$ and (c) $y = 0.20x + 0.80$, $R^2 = 0.58$. The range $VPD > 1$ was used for fitting in (c)

Mediterranean C3/C4 grassland (0.37–0.45) (Aires *et al*., 2008) and in a typical steppe in northern China (0.39–0.42) (Hao *et al*., 2007). Low *EF* may be characteristic of shrub ecosystems in northern China because of their arid climate and sparse vegetation. Maximum daily *ET* (3.3 mm day^{-1}, or λE of 7.9 MJ m^{-2} day^{-1}) at our site was comparable to the 3–4 mm day^{-1} observed in a semi-arid steppe in Inner Mongolia (Hao *et al*., 2007), a shrubland ecosystem in central New Mexico (Kurc and Small, 2004) and two semi-arid grasslands in Arizona (Krishnan *et al*., 2012). The biophysical controls on λE merit detailed investigation because of the close link between λE and eco-physiological processes (Baldocchi and Xu, 2007).

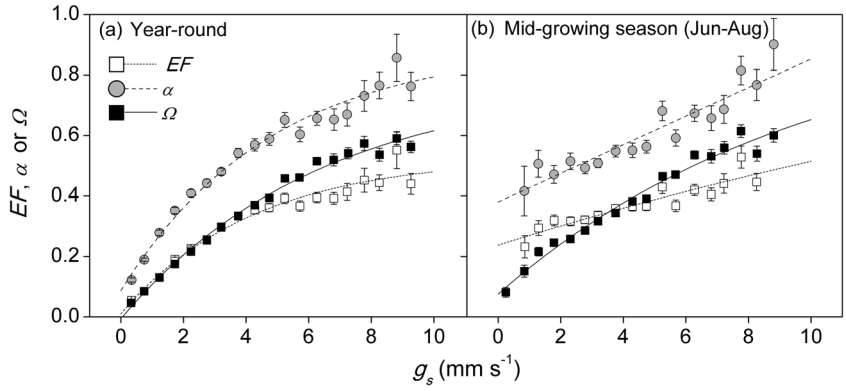

Figure 10. Effects of the bulk surface conductance (g_s) on evaporative fraction (EF), Priestley–Taylor coefficient (α) and decoupling coefficient (Ω) for (a) year-round measurements and (b) the mid-growing season (June–August), respectively, in 2012. Half-hourly values were bin-averaged into 0.5 mm s^{-1} g_s increments. Error bars refer to ±1 standard error. The regression curves for (a) are: EF, $y = 0.53 - 0.52\exp(-0.24x)$, $R^2 = 0.96$, α, $y = 0.90 - 0.81\exp(-0.21x)$, $R^2 = 0.98$, Ω, $y = 0.78 - 0.79\exp(-0.16x)$, $R^2 = 0.99$; and those for (b) are EF, $y = 1.20 - 0.96\exp(-0.03x)$, $R^2 = 0.85$, α, $y = 89.43 - 89.05\exp(-0.00053x)$, $R^2 = 0.88$, Ω, $y = 0.98 - 0.91\exp(-0.10x)$, $R^2 = 0.98$

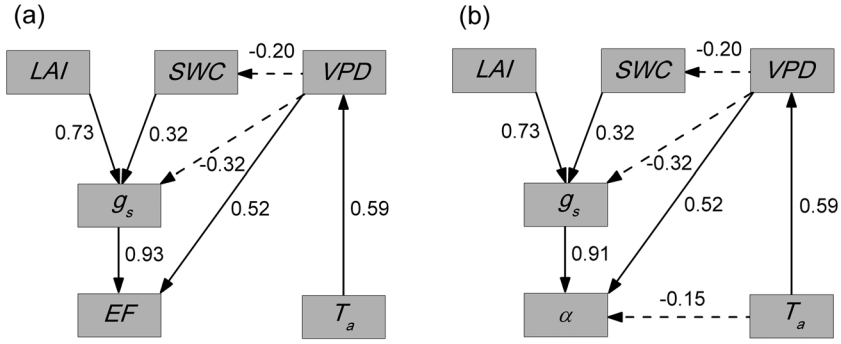

Figure 11. Final path diagrams for the effects of leaf area index (LAI), soil water content (SWC) at 30-cm depth, vapour pressure deficit (VPD), air temperature (T_a) and bulk surface conductance (g_s) on the (a) evaporative fraction (EF) and (b) Priestley–Taylor coefficient (α) in the growing season ($LAI > 0$) of 2012. Solid and dashed arrows represent positive and negative correlations, respectively. Standardized path coefficients are shown for each arrow

Surface controls: water availability and canopy phenology

Our results support our first hypothesis that water availability and canopy development are the primary factors affecting λE in semi-arid shrub ecosystems (Figures 6–9). Although there was a synchrony between the supply and demand for water, λE was often moisture-limited because of the large imbalance between annual ET_{eq} (692 mm) and PPT (~300 mm). During the mid-growing season, β decreased exponentially with soil moisture (Figure 9a), consistent with previous studies (Bracho *et al.*, 2008). EF (α) increased linearly from 0.30 (0.45) under dry conditions ($SWC = 0.06\,m^3\,m^{-3}$) to 0.5 (0.7) under wet conditions ($SWC = 0.16\,m^3\,m^{-3}$) (Figure 7a and b). In addition, the linear dependence of g_s and Ω on SWC (Figure 7c and d) suggested a strong stomatal control on ET and a tight canopy–atmosphere coupling under dry conditions (Li *et al.*, 2006; Liu and Feng, 2012). These results were qualitatively in line with previous studies of semi-arid grasslands, shrublands and steppes (Baldocchi *et al.*, 2004; Li *et al.*, 2006; Aires *et al.*, 2008; Krishnan *et al.*, 2012).

Unlike our results, many previous studies reported non-linear (e.g. asymptotic) responses of energy partitioning and canopy parameters to seasonal variations in soil water supply, with lower sensitivities at higher SWC (Baldocchi *et al.*, 2004; Aires *et al.*, 2008; Krishnan *et al.*, 2012; Ding *et al.*, 2013). This apparent discrepancy may partially be attributed to different SWC ranges being observed. For example, both Baldocchi *et al.* (2004) and Aires *et al.* (2008) found linear increases in α with SWC when soil was relatively dry ($SWC < 0.15\,m^3\,m^{-3}$). However, they reported a leveling off of α when $SWC \geq 0.15\,m^3\,m^{-3}$, a range well beyond our SWC records (Figure 7). Because reduced

sensitivities of *ET*-related parameters to *SWC* can be anticipated when water is ample, the linear relationships (Figure 7) indicated that the studied shrub ecosystem was always under water stress, even in a slightly wet year. The absence of any significant effect of *SWC* at depths other than 30 cm may be explained by the root distribution of dominant shrub species, which is concentrated primarily in the 20–50 cm soil layer (Wang *et al*., 2014). That is, the 0–10 cm layer was too shallow for root water uptake and thus contributed primarily to soil evaporation, whereas >70 cm was too deep for plant water use.

VPD imposes two opposite effects on λE. High *VPD* stimulates λE directly (see Equation (1)), however, this effect may be buffered or overwhelmed by *VPD*-induced stomatal closure. Negative effects of *VPD* on λE, *EF*, α and g_s have been well documented for water-limited ecosystems (Li *et al*., 2006; Baldocchi and Xu, 2007; Aires *et al*., 2008). Similarly, we found reduced g_s and Ω at high *VPD* (Figure 8c and d), indicating the importance of biotic regulation on transpiration (Krishnan *et al*., 2012). However, despite the decrease in g_s, both *EF* and α levelled off rather than declined at high *VPD* (Figure 8a and b). Such a lack of *VPD* response of α or *ET* has also been reported previously for different ecosystems (e.g. Ding *et al*., 2013; Tang *et al*., 2014). The direct positive effect of *VPD* on *ET* offset its negative effect on g_s, as indicated by our path analyses (Figure 11). Previous studies also illustrated such offsetting *VPD* effects during seasonal drought (Li *et al*., 2007; Tang *et al*., 2014). The increase in β with *VPD* (when *VPD* >1 kPa, Figure 9c) was probably associated with *VPD* responses by both *H* and λE (Li *et al*., 2009). The increasing trends of *EF*, α and g_s with *VPD* when *VPD* < 1 kPa (Figure 8a–c) have rarely been reported for semi-arid ecosystems. Baldocchi and Xu (2007) found in Mediterranean oak woodlands that an initial increase in *VPD* could enhance *ET*, although further increases in *VPD* will trigger a negative feedback on stomatal conductance, leading to reduced transpiration.

Canopy structure and *LAI* regulate energy partitioning via their impacts on surface albedo, roughness and stand transpiration (Li *et al*., 2006; Hammerle *et al*., 2008). Our results that *LAI* affected the seasonality of energy partitioning and bulk canopy parameters (Figures 6 and 11) were consistent with previous findings in semi-arid steppes and grasslands (Li *et al*., 2006; Hao *et al*., 2007; Krishnan *et al*., 2012). In addition, the monthly reference g_s at *VPD* of 1 kPa in the studied shrubland followed the seasonal pattern of *LAI* (data not shown), indicating that canopy phenology acted in concert with climatic factors to control the seasonal cycle of *ET*. The scattered relationships between *LAI* and canopy parameters (Figure 6) may be ascribed to the highly variable precipitation and soil moisture in semi-arid ecosystems that usually obscure *LAI* effects (Wang *et al*., 2008; Jia *et al*., 2014).

The direct control: surface conductance

The tight relationships of *EF* and α with g_s (Figure 10) were consistent with previous studies (Li *et al*., 2007; Krishnan *et al*., 2012; Liu and Feng, 2012), indicating strong physiological and phenological regulation of energy partitioning and *ET* in the studied shrubland. These relationships together with the path analyses (Figure 11) supported our second hypothesis that g_s strongly and directly affected energy partitioning and bulk canopy parameters. Moreover, neither *SWC* nor *LAI* showed any significant direct effect on *EF* and α (Figure 11); their controlling effects (Figures 6 and 7) were mediated through g_s. Based on our results, the energy partitioned to λE was largely controlled by the phenology of *LAI* and environmental regulation on g_s (Figure 11). Stomatal control over transpirational water loss is essential for the survival and growth of xerophytic shrub and grass species in water-limited environments (Li *et al*., 2006).

It is noteworthy that for the year-round relationships, the sensitivities of *EF* and α to g_s decreased with increasing g_s (Figure 10a). Such non-linear g_s responses have been observed in previous studies, suggesting an increasing degree of coupling between λE and available energy with higher g_s (Liu and Feng, 2012; Krishnan *et al*., 2012). However, *EF* and α were linearly correlated with g_s during the mid-growing period (Figure 10b), although g_s spanned a similar range (i.e. 0–10 mm s^{-1}). A saturation of α is expected with further increases in g_s. Both theoretical analysis and field data showed that α increased linearly with g_s over the range 0–10 mm s^{-1}, and then levelled off with further increases in g_s (Monteith, 1995).

SUMMARY AND CONCLUSIONS

We summarize our main findings as follows. First, *H* was the primary energy-balance component in the studied shrub ecosystem. λE exceeded *H* only during the mid-growing season. Second, *G* was also a major energy-balance component over daily and seasonal cycles but was negligible annually. Third, g_s imposed a dominant and direct control over λE. Both water availability and canopy development were important factors effecting g_s, and thus increases in *SWC* and *LAI* enhanced λE indirectly. Fourth, the direct effect of *VPD* on λE was buffered by the suppression of g_s with increasing *VPD*. These findings highlight the importance of adaptive plant

responses to water scarcity in regulating ecosystem energy partitioning. In addition, our results indicate the role that revegetation may play in the amelioration of local climate (e.g. by reducing β) and reversal of desertification in semi-arid areas.

Global climate models predict a more variable future precipitation regime with more extreme rainfall events punctuated by longer intervening dry periods (Thomey *et al*., 2011). Northern China may thus experience increases in drought frequency and intensity (Liu and Feng, 2012; Jia *et al*., 2014). Long-term studies are therefore needed to evaluate the effects of rainfall and soil moisture on the interannual variability of energy partitioning. In addition, future studies should focus on the response of g_s to climate change in relation to ecosystem energy partitioning, carbon uptake and water-use efficiency in semi-arid areas.

ACKNOWLEDGEMENTS

This study was supported by the National Natural Science Foundation of China (NSFC, proj. no. 31361130340, 31200537 and 31270755). It is also related to the ongoing Finnish–Chinese research collaboration project EXTREME, between Beijing Forestry University, School of Soil and Water Conservation (team led by Prof. Tianshan Zha) and University of Eastern Finland (UEF), School of Forest Sciences (team led by Prof. Heli Peltola), funded jointly by NSFC, the Academy of Finland and UEF (proj. no. 14921) for years 2013–2016. We are grateful to the reviewers and the Subject Editor for providing insightful comments and suggestions. We also thank Dr. Alan Barr for his help with language revision, and valuable comments on the manuscript. The U.S.–China Carbon Consortium (USCCC) promoted this work via helpful discussions and the exchange of ideas. H. S. Shi, Y. M. Zhang, X. W. Yang, S. J. Li, B. Wang and S. L. Tang assisted with field measurements and instrument maintenance.

REFERENCES

Aires LM, Pio CA, Pereira JS. 2008. The effect of drought on energy and water vapor exchange above a mediterranean C3/C4 grassland in Southern Portugal. *Agricultural and Forest Meteorology* **148**: 565–579. DOI:10.1016/j.agrformet.2007.11.001.

Asner GP, Archer S, Hughes RF, Ansley RJ, Wessman CA. 2003. Net changes in regional woody vegetation cover and carbon storage in Texas Drylands, 1937–1999. *Global Change Biology* **9**: 316–335. DOI:10.1046/j.1365-2486.2003.00594.x.

Baldocchi DD, Xu L. 2007. What limits evaporation from Mediterranean oak woodlands—the supply of moisture in the soil, physiological control by the plants or the demand by the atmosphere? *Advances in Water Resources* **30**: 2113–2122. DOI:10.1016/j.advwatres.2006.06.013.

Baldocchi DD, Xu L, Kiang N. 2004. How plant functional-type, weather, seasonal drought, and soil physical properties alter water and energy fluxes of an oak-grass savanna and an annual grassland. *Agricultural and Forest Meteorology* **123**: 13–39. DOI:10.1016/j.agrformet.2003.11.006.

Barr AG, Morgenstern K, Black TA, McCaughey JH, Nesic Z. 2006. Surface energy balance closure by the eddy-covariance method above three boreal forest stands and implications for the measurement of the CO_2 flux. *Agricultural and Forest Meteorology* **140**: 322–337. DOI:10.1016/j.agrformet.2006.08.007.

Bourque CPA, Hassan QK. 2009. Vegetation control in the long-term self-stabilization of the Liangzhou Oasis of the Upper Shiyang River watershed of west-central Gansu, northwest China. *Earth Interactions* **13**: 1–22. DOI:10.1175/2009EI286.1.

Bracho R, Powell TL, Dore S, Li J, Hinkle CR, Drake BG. 2008. Environmental and biological controls on water and energy exchange in Florida scrub oak and pine flatwoods ecosystems. *Journal of Geophysical Research* **113**: G02004. DOI:10.1029/2007JG000469.

Burba G. 2013. *Eddy Covariance Method for Scientific, Industrial, Agricultural and Regulatory Applications*. LI-COR Biosciences: Lincoln, USA.

Chen X, Duan Z. 2009. Changes in soil physical and chemical properties during reversal of desertification in Yanchi County of Ningxia Hui autonomous region, China. *Environmental Geology* **57**: 975–985. DOI:10.1007/s00254-008-1382-1.

Ding R, Kang S, Li F, Zhang Y, Tong L. 2013. Evapotranspiration measurement and estimation using modified Priestley–Taylor model in an irrigated maize field with mulching. *Agricultural and Forest Meteorology* **168**: 140–148. DOI:10.1016/j.agrformet.2012.08.003.

Feng W, Zhang Y, Jia X, Wu B, Zha T, Qin S, Wang B, Shao C, Liu J, Fa K. 2014. Impact of environmental factors and biological soil crust types on soil respiration in a desert ecosystem. *PLoS ONE* **9**: e102954. DOI:10.1371/journal.pone.0102954.

Gao Y, Li X, Liu L, Jia R, Yang H, Li G, Wei Y. 2012. Seasonal variation of carbon exchange from a revegetation area in a Chinese desert. *Agricultural and Forest Meteorology* **156**: 134–142. DOI:10.1016/j.agrformet.2012.01.007.

Hammerle A, Haslwanter A, Tappeiner U, Cernusca A, Wohlfahrt G. 2008. Leaf area controls on energy partitioning of a temperate mountain grassland. *Biogeosciences* **5**: 421–431. DOI:10.5194/bg-5-421-2008.

Hao Y, Wang Y, Huang X, Cui X, Zhou X, Wang S, Niu H, Jiang G. 2007. Seasonal and interannual variation in water vapor and energy exchange over a typical steppe in Inner Mongolia, China. *Agricultural and Forest Meteorology* **146**: 57–69. DOI:10.1016/j.agrformet.2007.05.005.

Heusinkveld BG, Jacobs AFG, Holtslag AAM, Berkowicz SM. 2004. Surface energy balance closure in an arid region: role of soil heat flux. *Agricultural and Forest Meteorology* **122**: 21–37. DOI:10.1016/j.agrformet.2003.09.005.

Jarvis PG, McNaughton KG. 1986. Stomatal control of transpiration: scaling up from leaf to region. *Advances in Ecological Research* **15**: 1–49.

Jia X, Zha TS, Wu B, Zhang YQ, Gong JN, Qin SG, Chen GP, Qian D, Kellomäki S, Peltola H. 2014. Biophysical controls on net ecosystem CO_2 exchange over a semi-arid shrubland in northwest China. *Biogeosciences* **11**: 4679–4693. DOI:10.5194/bg-11-4679-2014.

Krishnan P, Meyers TP, Scott RL, Kennedy L, Heuer M. 2012. Energy exchange and evapotranspiration over two temperate semi-arid grasslands in North America. *Agricultural and Forest Meteorology* **153**: 31–44. DOI:10.1016/j.agrformet.2011.09.017.

Kurc SA, Small EE. 2004. Dynamics of evapotranspiration in semiarid grassland shrubland ecosystems during the summer monsoon season, central New Mexico. *Water Resources Research* **40**: W09305. DOI:10.1029/2004WR003068.

Launiainen S. 2010. Seasonal and inter-annual variability of energy exchange above a boreal Scots pine forest. *Biogeosciences* **7**: 3921–3940. DOI:10.5194/bg-7-3921-2010.

Li SG, Eugster W, Asanuma J, Kotani A, Davaa G, Oyunbaatar D, Sugita M. 2006. Energy partitioning and its biophysical controls above a grazing steppe in central Mongolia. *Agricultural and Forest Meteorology* **137**: 89–106. DOI:10.1016/j.agrformet.2006.03.010.

Li SG, Asanuma J, Kotani A, Davaa G, Oyunbaatar D. 2007. Evapotranspiration from a Mongolian steppe under grazing and its environmental constraints. *Journal of Hydrology* **333**: 133–143. DOI:10.1016/j.jhydrol.2006.07.021.

Li Y, Zhou L, Xu Z, Zhou G. 2009. Comparison of water vapor, heat and energy exchanges over agricultural and wetland ecosystems. *Hydrological Processes* **23**: 2069–2080. DOI:10.1002/hyp.7339.

Liu H, Feng J. 2012. Seasonal and interannual variations of evapotranspiration and energy exchange over different land surfaces in a semi-arid area of China. *Journal of Applied Meteorology and Climatology* **51**: 1875–1888. DOI:10.1175/JAMC-D-11-0229.1.

Liu R, Li Y, Wang QX. 2011. Variations in water and CO_2 fluxes over a saline desert in western China. *Hydrological Processes* **26**: 513–522. DOI:10.1002/hyp.8147.

Monteith JL. 1965. Evaporation and environment. In *The State and Movement of Water in Living Organisms*, Fogg GE (ed). Academic Press: New York; 205–234.

Monteith JL. 1995. Accommodation between transpiring vegetation and the convective boundary layer. *Journal of Hydrology* **166**: 251–263. DOI:10.1016/0022-1694(94)05086-D.

Monteith JL, Unsworth MH. 1990. *Principles of Environmental Physics*. Butterworth-Heinemann: Oxford.

Ochsner TE, Sauer TJ, Horton R. 2007. Soil heat storage measurements in energy balance studies. *Agronomy Journal* **99**: 311–319. DOI:10.2134/agronj2005.0103S.

Papale D, Reichstein M, Aubinet M, Canfora E, Berhofer C, Kutsch W, Longdoz B, Rambal S, Valentini R, Vesala T, Yakir D. 2006. Towards a standardized processing of Net Ecosystem Exchange measured with eddy covariance technique: algorithms and uncertainty estimation. *Biogeosciences* **3**: 571–583. DOI:10.5194/bg-3-571-2006.

Poulter B, Frank D, Ciais P, Myneni RB, Andela N, Bi J, Broquet G, Canadell JG, Chevallier F, Liu YY, Running SW, Sitch S, van der Werf GR. 2014. Contribution of semi-arid ecosystems to interannual variability of the global carbon cycle. *Nature* **509**: 600–603. DOI:10.1038/nature13376.

Priestley CHB, Taylor RJ. 1972. On the assessment of surface heat flux and evaporation using large-scale parameters. *Monthly Weather Review* **100**: 81–92. DOI:10.1175/1520-0493(1972)100<0081:OTAOSH>2.3.CO;2.

Tang Y, Wen X, Sun X, Zhang X, Wang H. 2014. The limiting effect of deep soil water on evapotranspiration of a subtropical coniferous plantation subjected to seasonal drought. *Advances in Atmospheric Sciences* **31**: 385–395. DOI:10.1007/s00376-013-2321-y.

Thomey ML, Collins SL, Vargas R, Johnson JE, Brown RF, Natvig DO, Friggens MT. 2011. Effects of precipitation variability on net primary production and soil respiration in a Chihuahuan Desert grassland. *Global Change Biology* **17**: 1505–1515. DOI:10.1111/j.1365-2486.2010.02363.x.

Wang Y, Zhou G, Wang Y. 2008. Environmental effects on net ecosystem CO2 exchange at half-hour and month scales over Stipa krylovii steppe in northern China. *Agricultural and Forest Meteorology* **148**: 714–722. DOI:10.1016/j.agrformet.2008.01.013.

Wang B, Zha TS, Jia X, Wu B, Zhang YQ, Qin SG. 2014. Soil moisture modifies the response of soil respiration to temperature in a desert shrub ecosystem. *Biogeosciences* **11**: 259–268. DOI:10.5194/bg-11-259-2014.

Wilson K, Goldstein A, Falge E, Aubinet M, Baldocchi D, Berbigier P, Bernhofer C, Ceulemans R, Dolman H, Field C, Grelle A, Ibrom A, Law BE, Kowalski A, Meyers T, Moncrieff J, Monson R, Oechel W, Tenhunen J, Valentini R, Verma S. 2002. Energy balance closure at FLUXNET sites. *Agricultural and Forest Meteorology* **113**: 223–243. DOI:10.1016/S0168-1923(02)00109-0.

Zha T, Kelloäki S, Wang KY, Rouvinen I. 2004. Carbon sequestration and ecosystem respiration for 4 years in a Scots pine forest. *Global Change Biology* **10**: 1492–1503. DOI:10.1111/j.1365-2486.2010.02363.x.

Zha T, Li C, Kellomäki S, Peltola H, Wang KY, Zhang Y. 2013. Controls of evapotranspiration and CO_2 fluxes from Scots Pine by surface conductance and abiotic factors. *PLoS ONE* **8**: e69027. DOI:10.1371/journal.pone.0069027.

APPENDIX TABLE A1: NOMENCLATURE

Abbreviations/ symbols	Description
C_p	Specific heat capacity of air ($J\,kg^{-1}\,K^{-1}$)
EF	Evaporative fraction ($\lambda E/R_n$)
ET	Evapotranspiration (mm)
ET_{eq}	Equilibrium ET (mm)
g_a	Aerodynamic conductance ($m\,s^{-1}$)
g_s	Bulk surface conductance ($m\,s^{-1}$)
G	Total soil heat flux ($G_{10\text{-}cm}+S_b$, $W\,m^{-2}$, $MJ\,m^{-2}\,day^{-1}$)
$G_{10\text{-}cm}$	Soil heat flux measured at 10-cm depth ($W\,m^{-2}$)
H	Sensible heat flux ($W\,m^{-2}$, $MJ\,m^{-2}\,day^{-1}$)
LAI	Leaf area index ($m^2\,m^{-2}$)
RH	Relative humidity of the air (%)
R_n	Net radiation ($W\,m^{-2}$)
R_s	Shortwave global solar radiation ($W\,m^{-2}$, $MJ\,m^{-2}\,day^{-1}$)
S_a	Aboveground heat storage ($S_{\lambda E}+S_H$, $W\,m^{-2}$)
S_b	Soil heat storage change above the soil heat plates ($W\,m^{-2}$)
S_H	Sensible heat storage in the air column below the EC instrument height ($W\,m^{-2}$)
$S_{\lambda E}$	Latent heat storage in the air column below the EC instrument height ($W\,m^{-2}$)
SWC	Soil water content ($m^3\,m^{-3}$)
T_a	Air temperature (°C)
T_{a_max}	Daily maximum T_a (°C)
T_{a_min}	Daily minimum T_a (°C)
u	Wind speed ($m\,s^{-1}$)
u^*	Friction velocity ($m\,s^{-1}$)
VPD	Vapour pressure deficit (kPa)
α	Priestley–Taylor coefficient ($\lambda E/\lambda E_{eq}$)
β	Bowen ratio ($H/\lambda E$)
γ	Psychrometric constant ($kPa\,K^{-1}$)
Δ	Slope of the saturation vapour pressure *versus* T_a curve ($kPa\,K^{-1}$)
λE	Latent heat flux ($W\,m^{-2}$, $MJ\,m^{-2}\,day^{-1}$)
λE_{eq}	Equilibrium λE ($W\,m^{-2}$, $MJ\,m^{-2}\,day^{-1}$)
ρ	Air density ($kg\,m^{-3}$)
Ω	Decoupling coefficient